Spectral computed tomography in cardiology

Vu Tuan Nguyen [1]✉, Viet Lan Nguyen [2]

[1] Pham Ngoc Thach University of Medicine

[2] Vietnam National Heart Institute, Bach Mai Hospital

ABSTRACT

Cardiac computed tomography (CT) has become a valuable tool in the equipment of the cardiologist. Many technological advances in CT have occurred recently, including dual-energy CT (DECT) or spectral CT. CT is now considered a reliable tool to assess coronary artery stenosis, but it still has two main areas for improvement. Firstly, difficult estimation of the degree of stenosis in the presence of calcified plaque; secondly, CT needs to be improved in correctly identifying plaque components. Spectral CT permits accurate plaque characterization, assessment of myocardial perfusion, acute myocarditis, non-ischemic dilated cardiomyopathy, determining if shadowing inside a stent is an artifact or restenosis, better delineation of aortic stent graft endoleaks, detection of both acute and chronic pulmonary embolisms. Also, lower contrast and radiation doses of 50-60% and even 90% in some studies.

Currently, both transesophageal ultrasound (TEE) and CT evaluations are necessary before AF ablation. The TEE evaluation reveals that the cardiac thrombi and multislice CT anatomic reconstructions of the left atrium and pulmonary veins guide the isolation procedure.

Keywords: Dual-energy CT, Spectral CT.

I. OVERVIEW

Principles of computed tomography

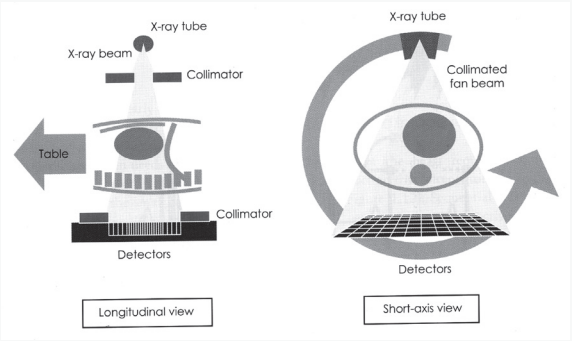


Figure 1.1. Principles of computed tomography. Source: "Pim J de Feyter 2005"(1)

The X-ray tube's beam decreases in intensity as it passes through the body. The unit of measurement for that decrease is the Hounsfiel, abbreviated as HU. Detectors facing the X-ray tube will detect the reduction in intensity, transmit it to the computer's processing system, digitalize the data, and generate a basic cross-sectional image. (Axial source images), the captured structures are re-rendered base on the HU. Data acquisition is usually taken at the end of diastole, e.g., 60% from the preceding R wave. (1)

Correspondence to: Dr. Vu Tuan Nguyen. Pham Ngoc Thach University of Medicine, Ho Chi Minh City, Vietnam. Email: tuanvu2401@gmail.com

Spiral CT was introduced in 1990 with continuously rotating X-ray tubes and a bed moving constantly. This configuration significantly reduced the total scan time but needed to be faster for cardiac scanning. Multi-Slice Computed Tomography (MSCT) or now more commonly known as multi-sensor tomography, also known as Multidetector Computed Tomography MDCT, was introduced in 1998 with four detectors; in 2002, there were 16 detectors; in 2004, 64 detectors, then 128, 256, and 320 respectively, and now 640 detectors (640 - Slice Multidetector Computed tomography). With a 320 or 640 sensor, 0.5mm thin slices can be captured, and a Gantry rotation time as short as 0.33 seconds, thus providing enough temporal and spatial resolution to capture the heart and coronary angiography in just one turn of the X-ray tube (2), (3), (4)

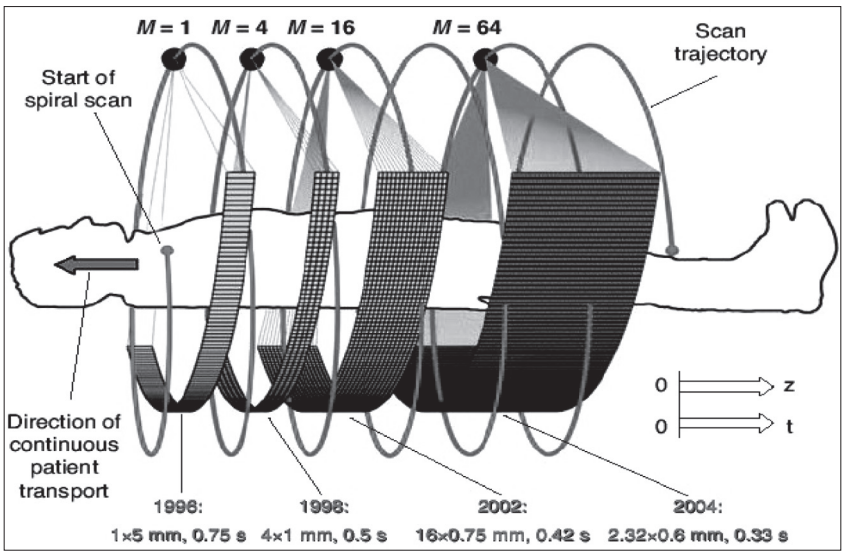


Figure 1.2. Spiral CT và MSCT. (Source: U. Joseph Schoepf 2005) (5)

Spectral Computed Tomography

Spectral CT has received much attention in recent years and is also one of the most interesting topics at the annual meeting of the American Society of Cardiac CT 2019 (Society of Cardiac Computed Tomography 2019). Dual-Energy Computed Tomography represents the latest significant advancement in the field of CT. This technique detects morphology and helps distinguish the chemical composition of examined tissue structures, bringing CT into the functional assessment of organs. This method obtains images that occur at the same or near the same time at low and high energies (kilovolt peaks) (80 kVp and 140kVp). Different energy levels allow the control of two polychromatic spectra to distinguish the densities of two different matters. (6),(7),(8),(9)

The photoelectric effect that produces images depends strongly on the X-ray's photon energy, the nuclear charge Z of the matter, or the binding energy of the electron layer closest to the nuclear, called the K shell. We can distinguish different substances based on the difference in K shell bonding energy at different energies between 80 kVp and 140 kVp. (6),(7),(8),(9)

Principles of Spectral Computed Tomography

Dual-Source Scanner with Dual Detector Arrays:

Siemens Healthcare. (10) Dual-energy CT with one X-ray tube with two energy sources or capable of fast kilovoltage (KV) switching between high and low KV (Single-Source Scanner with Fast Kilovoltage Switching): Canon, GE Healthcare.(10) Single-Source Scanner with Dual Detector Layers: Philips Healthcare.

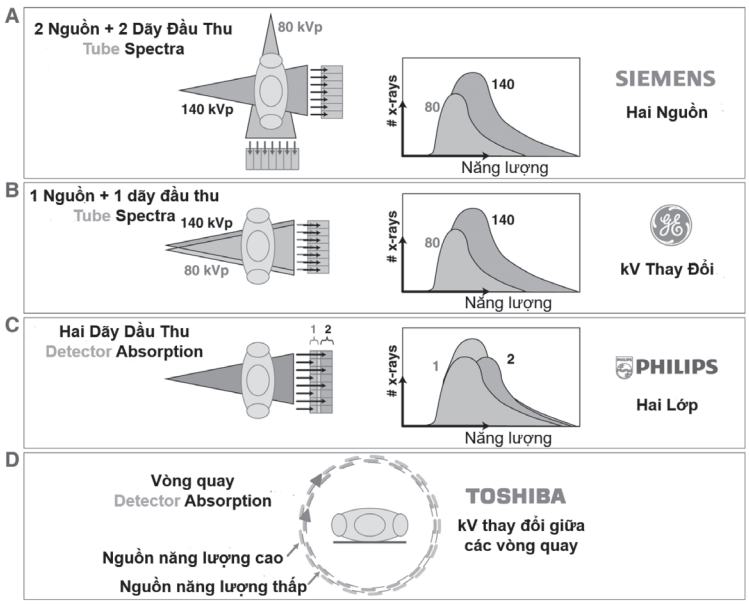


Figure 1.3. Types of spectral computed tomography configuration. (A) Paired detectors with each source operating at a different voltage. Each X-ray source covers a different scanning field. (B) An X-ray source capable of rapidly switching voltages in one revolution. (C) Sensor with two layers made of 2 different materials capable of distinguishing between low energy (upper layer) and high energy (lower layer) photons, with the source operating at a constant voltage. (D) A source-sensor pair with a sequential switching source voltage. (Source: J Am Coll Cardiol Img. 2015 Jun, 8 (6) 710–723)(10)

II. APPLICATIONS OF SPECTRAL COMPUTED TOMOGRAPHY IN CARDIOLOGY

Computed tomography spectrum not only evaluates the degree of coronary artery stenosis but also determines the degree of risk of atherosclerosis, assesses myocardial perfusion, myocarditis, and cardiomyopathy, monitors the function of coronary stents after the intervention, evaluation aortic Graft stents, detecting acute and chronic pulmonary embolism. In addition, the CT spectrum also helps in the differential diagnosis of thrombus or tumors in the heart chambers and investigates mechanical valve movements by reducing artifacts. (10)

1. Evaluating myocardial perfusion

Evaluation of myocardial perfusion is the most valuable application of Spectral Computed Tomography in cardiology. Using contrast may show different pharmacokinetics between normal, ischemic, and infarcted myocardium regions because most tissues, including the myocardium, are mostly water. Reconstruction of water-suppression imaging from dual-energy CT will allow quantification of Iodine and possibly quantification of myocardial perfusion. Myocardial perfusion imaging and Iodine mapping assist in CT spectroscopy as a functional diagnostic test to help guide treatment. (8),(10),(11).

Multiple modalities for assessing myocardial perfusion include resting only (without vasodilators), pre-exercise phase with vasodilators (Adenosine, Dipirydamol, Regadenoson), followed by stress-rest, and vice versa. All images during the exercise and rest periods allow the assessment of fixed and reversible perfusion defects. In the assessment of myocardial perfusion by CT, according to the consensus of the American Heart Association in 2020, the assessment of myocardial perfusion defects is assessed visually by the American Heart Association's 17-partition model: a) Severity: whether hypoperfusion is present (binary). b) Size: The size of the perfusion defect area (small, moderate, or large) as well as the transmural (>50%) or non-transmural (<50%) perfusion defect. The transmural perfusion ratio (TPR) was calculated by dividing the mean HU concentration in the subendocardial area by the subendocardial HU density. In the mean epicardial, if TPR < 1 is abnormal, if TPR < 0.75, is highly suggestive of myocardial ischemia. c) Reversibility. According to the recommendations of the American Heart CT Society 2020, perform myocardial perfusion assessment in combination with contrast-enhanced CT angiography for patients with a high risk of ischemic heart disease, known coronary artery disease, and intervention previously, moderate coronary artery stenosis, significant coronary calcification. (8),(10),(11).

Spectral CT provides good results in assessing myocardial perfusion compared to imaging methods considered gold standards, such as cardiac MRI and SPECT. According to Meinel et al., compared with SPECT, the CT spectrum is capable of assessing myocardial perfusion with a sensitivity of 92% and a specificity of 98% if only the resting phase is performed (rest scan), and if it is performed both the stress scan combined with the resting phase (rest scan) and the late enhancement phase (Late Enhancement), the accuracy increased significantly: sensitivity 99% and specificity 97%. These results suggest that CT spectroscopy to evaluate myocardial perfusion during rest and exercise should be considered the first choice for myocardial perfusion study. (8),(11)

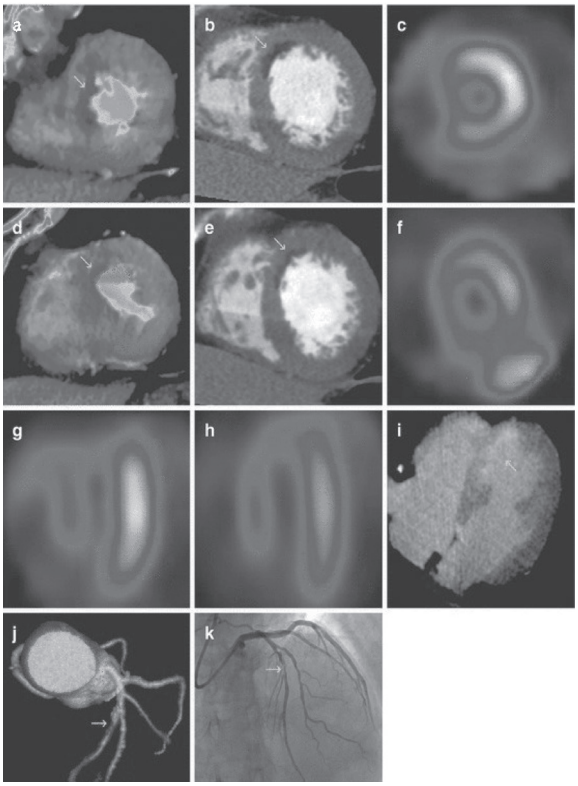


Figure 2.1. Myocardial necrosis in a 68-year-old male patient. Cardiovascular risk factors: dyslipidemia. History of gastritis, acute chest pain with negative cardiac enzymes and normal ECG. In 2010, the patient had a SPECT performed which showed normal results. The patient continued to have chest pain. A dual-energy CT scan with exercise and rest mapping iodine color and grayscale at 70 keV shows a fixed subendocardial perfusion defect in the anterior wall of the septum (arrows)(a,b,d,e).). Exercise–rest SPECT imaging also had similar findings (c, f). SPECT image at exercise and at rest in a four-chamber view from

the apex shows a fixed defect in the anterior septum (g,h). Two-energy CT image in late enhancement: shows enhancement of the anterior wall corresponding to the area of myocardial necrosis (arrow) (i). Three-dimensional reconstruction of the coronary tree shows severe LAD stenosis. in paragraph 7 (arrow) (j) and similar invasive coronary angiography (k). (Source: Carrascosa, P. M., & Cury, R. C. (2015) Myocardial Perfusion by Dual Energy CT. Dual -Energy CT in Cardiovascular Imaging.) (8)

2. Diagnosis of myocardiopathy

Delayed Myocardial Enhancement is considered a marker of myocardial fibrosis or scarring and is an essential feature in the assessment of MI and myocardial survival and in the evaluation of cardiomyopathy not due to ischemia. (12)

Compared with cardiac MRI, considered the gold standard in evaluating late contrast enhancement, CT spectrum has a sensitivity of 72-77% and a specificity of 88-92% in the evaluation of older MI, which is significantly higher than conventional CT images. In addition, late contrast enhancement on the CT spectrum can also detect non-ischemic cardiomyopathy. (12)

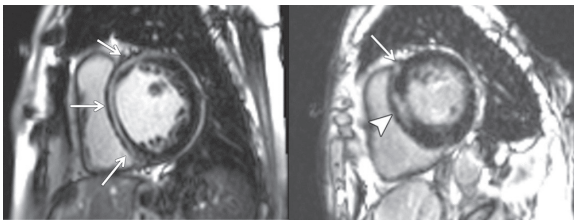


Figure 2.2. Late contrast enhancement in the mid-myocardium in patients with dilated cardiomyopathy and late contrast in the interventricular septum and biventricular junction in patients with hypertrophic cardiomyopathy. (Source: Ohta, Y. et al. (2018) Myocardial delayed enhancement CT for the evaluation of heart failure: comparison to MRI Radiology, 288(3), 682-691.)(12)

3. Diagnosis of acute myocarditis.

Spectral CT is a new technique for diagnosing acute myocarditis based on late iodine enhancement. In a study that compared with cardiac MRI in the diagnosis of acute myocarditis, it was found that spectral CT had a very high sensitivity of 100% based on patient analysis and a sensitivity of 82% for region-specific comparisons of 99%, positive predictive value 94%, negative predictive value 95%, and the concordance between these two methods is very high, with Kappa coefficient = 0.84. (13)

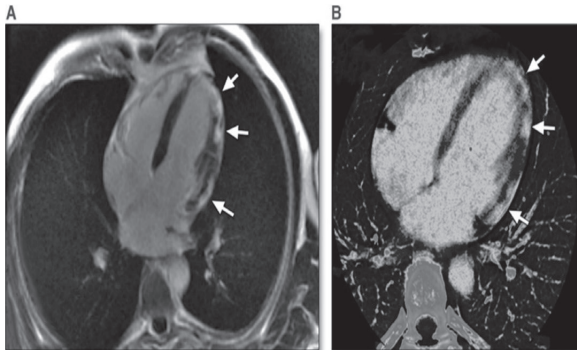


Figure 2.3. Late administration of gadolinium (Late Gadolinium Enhancement) in a 4-chamber view on cardiac MRI shows subepicardial myocarditis in the lateral wall and left ventricular apex (A). Similarly, the CT spectrum shows late enhancement with Iodine (B). (Source: Adeboye, A. et al. (2022). A review of the role of imaging modalities in evaluating viral myocarditis with a special focus on COVID-19-related myocarditis. Diagnostics, 12(2), 549.) (14)

4. Removal of calcifications in the assessment of atherosclerosis causing coronary stenosis

The monochromatic analysis allows anatomical visualization at energies ranging from 40 to 140 keV. Different grades show luminosity and atheroma with different intensities, areas, and volumes. With spectroscopic computed tomography, the artifact due to calcification was significantly reduced. (15)

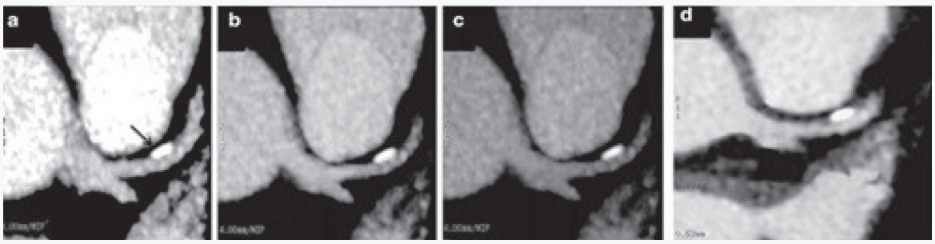


Figure 2.4. Dual-energy CT: atheroma with calcification proximal to LAD, large plaque at 40keV (a), a smaller plaque at 60keV (b), and atheroma further reduced in size at 80keV (c). On one-energy CT: atheroma with calcifications equal in size to that of 60keV (d). (Source: Carrascosa PM, Cury RC. Dual-Energy CT in Cardiovascular Imaging. 2015:173-230.)(15)

5. Diagnosis of high-risk plaque

High-risk plaque (HRP) was formerly known by another term vulnerable plaque.(16) Data from recent coronary CT studies described HRP features that are associated with an increased likelihood of future acute coronary syndromes and ischemia. HRP features include positive remodeling, low-density plaque, microcalcifications, and a donut-shaped sign (Napkin's ring).(16) These atheroma features are detected by Intravascular echocardiography and histological features of advanced atherosclerotic plaque and thin-encapsulated atherosclerotic plaque, potentially progressing to atheroma rupture/ thrombosis. (16)

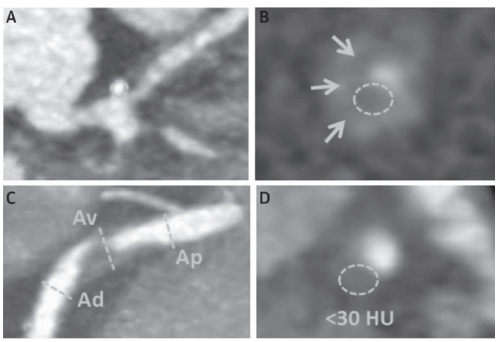


Figure 2.5. Types of high-risk atherosclerotic plaques. A: Spotty calcification. B: Napkin-ring sign. C: Positive remodeling. D: Low density (< 30 HU). (Source: Cury, R. C. et al. (2022). Cardiovascular Imaging, 15(11), 1974-2001.)(16)

6. Assessment of coronary stents after intervention

Computed tomography (CT) is a noninvasive diagnostic method that helps evaluate the lumen of the stent through the recognition of clear contrast material in the lumen downstream of the stent. (17)

However, this may be limited for stents that are small in size or contain a lot of metal due to the blurring phenomenon (Blooming artifact). Thanks to the CT spectrum scanner and the incident X-ray photon energy level adjustment, we can remove the stent or calcification to investigate whether the stent is blocked. The software of the CT spectrum machine has a pair of Calcium and Iode. When scanning, it can remove Calcium and get an Iode signal. (17)

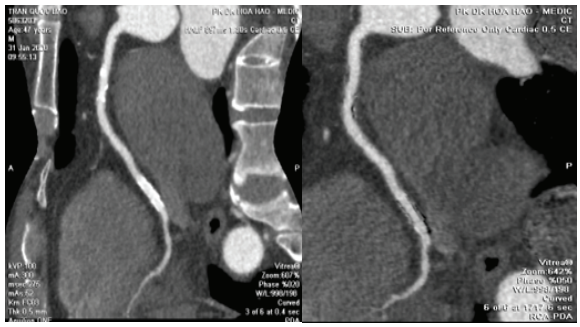


Figure 2.6. RCA distal stent, after stent removal and calcium, clearly see and evaluate the stent lumen. (Source: TTYK Medic 2021).

7. Detecting Graft stent endoleak in the aorta

Spectral CT also plays an important role in evaluating the endoleak after the stenting of the aorta in patients with aortic dissection, which is difficult for conventional CT because of the effects of metal artifacts and patient exposure to high radiation. Spectral CT provides virtual non-contrast images from arterial or venous phase data and thus reduces radiation exposure by nearly 50%. Phased venous CT angiography and virtual non-contrast datasets have been evaluated in multiple studies for patients following the repair of an aortic aneurysm. Algorithms are helpful for the fast and accurate evaluation of two-energy aortic data: virtual non-contrast images, iodine maps, and hard plaque algorithms are used to distinguish between Iodine and calcium. (18)

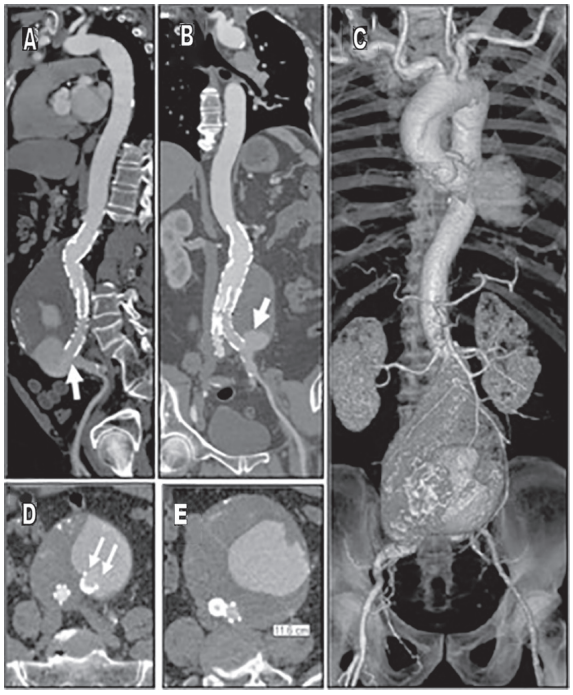


Figure 2.7. MDCT 320 showing a leaky abdominal aortic stent (arrow) (Source: Kassem TW. The Egyptian Journal of Radiology and Nuclear Medicine. 2017;48(3):621-6.)](19)

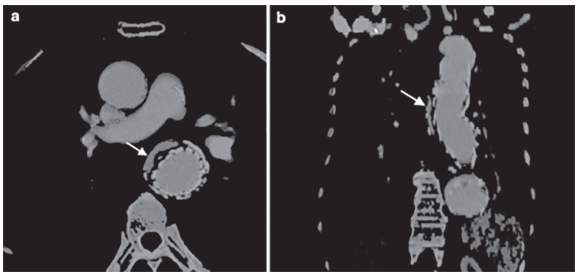


Figure 2.8. Axial (a) and coronal (b) slices show that Iodine (blue) is detected in the aneurysm and outside the Graft Stent. This corresponds to a type I endovascular fistula derived from the distal end of the Stent Graf. (Source: Sommer WH. Aorta Dual Energy CT in Clinical Practice. 2011:61-6.)(18)

8. Diagnosis of pulmonary embolism

Spectral CT of pulmonary arteries shows pulmonary embolism in the major branches, the segmental or subsegmental branches, and the corresponding hypoperfusion area on the coding image colorimetry. (20) Lysdahlgaard, S., Hess, S., Gerke, O., et al., in a comparative study between computed tomography and perfusion scintigraphy (V/Q Scan) published in the European Radiology journal, showed that the sensitivity, specificity, positive predictive value and negative predictive value of CT spectrum were 94.2% (95% CI, 88.3–100%), respectively 88.5% (95% CI, 81.3–95.6%), 87.8% (95%CI, 80.3–95.4%) and 94.5% (95%CI, 89.3–99.7%). (18)

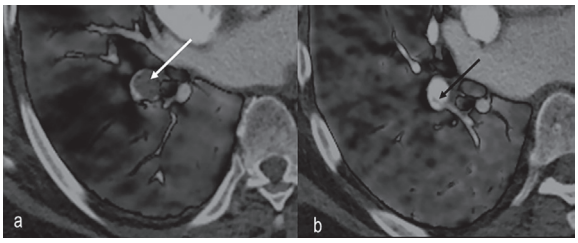


Figure 2.9. Image of pulmonary artery thrombosis. Initial evaluation with dual-energy CT shows a right lower lobe embolism (arrow) with pulmonary peripheral perfusion defect (a). Photographs taken

14 months later revealed that the embolus had almost completely disappeared but with some residual vascular defect (b). (Source: Vlahos, I. et al (2022). Dual-energy CT in pulmonary vascular disease. The British Journal of Radiology, 95(1129), 20210699.).(20)

9. Diagnosis of cardiac tumor

Although space-occupying lesions (thrombus or tumors) in the heart are uncommon, they carry a high risk of embolism, so an accurate and timely diagnosis is essential. Differentiating cardiac tumors from cardiac thrombosis is essential because of different treatment strategies. Spectral CT and MRI are good diagnostic tools. (21) According to Yoo Jin Hong et al., in a study analyzing the characteristics: of HU (CT attenuation value) of the mass during the arterial and late phase as well as Iodine concentration (mg/ml) on dual-energy CT and signal intensity ratio (SI) on cardiac MRI of intracardiac thrombus, cardiac tumor to evaluate the diagnostic value of dual-energy CT to differentiate between cardiac tumor and thrombosis. When Iodine concentration was used to differentiate between thrombosis and cardiac tumor, the optimal cut-off value for Iodine concentration for discriminating between thrombosis and heart tumor was 2.55 mg/ml, with a sensitivity of 66.7% and specificity of 79%. The area under the ROC curve of iodine concentration (mg/ml) was 0.77 (95%CI: 0.63-0.91) higher than the area under the ROC curve of HU concentration after injection. The contrast was 0.51 (95%CI: 0.34-0.69), and there was a statistically significant difference between the area under the ROC curve of iodine concentration and HU concentration after contrast injection $p < 0.001$ (AUC: -0.38, 95%CI: −0.49 – −0.27, $p < 0.001$) and the area under the ROC curve of the SI ratio on cardiac MRI is 0.89 significantly higher than the area under the ROC curve of iodine concentration (AUC; 0.77 vs. 0.89; $p = 0.04$). (21)

Table 2.1. Differences Between Heart Tumor and Thrombosis [21]

	Cardiac tumor (n=24)					Thrombosis (n=19)	P
	Lymphoma (n=4)	Metastasis (n=5)	Myxoma (n=9)	Other tumors* (n=6)	All		
Volume (cm^3)	32,14 ± 8,77	36,5±7,84	24,24 ± 5,84	9,89 ± 7,16	24,52 ± 3,76	3,98 ± 4,22	<0,001
attenuation HU	94,63 ± 21,1	88,6 ± 18,88	74,11±14,08	44,02 ±17,24	73,03 ±8,78	74,5 ± 9,87	0,912
Iodine concentration (mg/ ml)	3,04 ± 0,58	2,96 ± 0,52	3,33 ± 0,39	2,43 ± 0,47	2,98 ± 0,23	1,79 ± 0,26	0,002
SI ratio	4,13 ± 2,76	3,31 ± 3,39	10,3 ± 1,95	5,92 ± 2,14	6,9 ± 0,12	1,43 ± 0,14	0,008

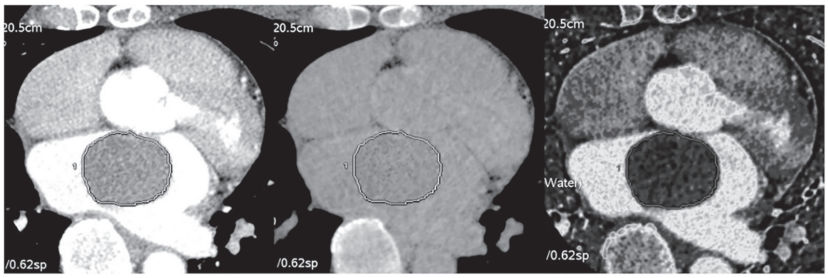


Figure 2.10. Quantitative analysis image on dual energy CT of the heart tumor. (A) 70keV monochromatic image represents the post-contrast CT image, (B) the de-Iodine image represents the pre-contrast CT image, and (C) the Iodine panel image. (Source: Hong, Y. J. et al. (2018). Scientific reports, 8(1), 15334.)(21)

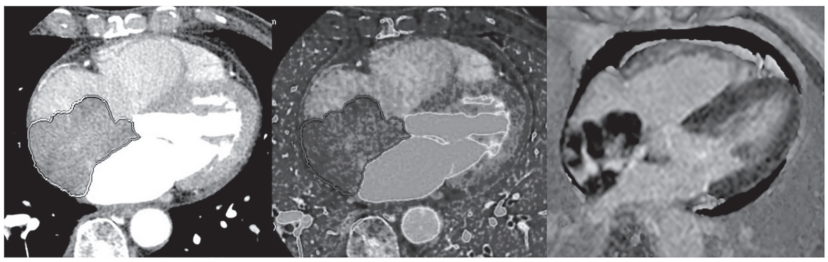


Figure 2.11. Right atrial lymphoma. (a) Contrast-enhanced spectral CT shows a 68 mm x 48 mm multilobed mass in the right atrium. Volume 47.1cm^3, density 70HU, (b) Iodine chart showing that Iodine concentration in this volumetric volume (VOI) is 1.67mg/ml, (c) Cardiac MRI 3 days later, start contrast agent late (LGE) showed this mass with increased central enhancement, SI ratio of 4.16, small pericardial effusion. (Source: Hong, Y. J. et al. (2018). Scientific reports, 8(1), 15334.)(21)

10. Investigation of left atrial thrombosis and mapping of anatomical correlation before atrial fibrillation ablation

In a study of 63 patients, 13 thrombosis and 19 cases of spontaneous echogenicity or spontaneous echo contrast (SEC) were detected by esophageal echocardiography (SATTQ). Using SATTQ as a reference standard, the sensitivity, specificity, positive predictive value, and negative predictive value of two-energy cardiac CT in detecting thrombosis and SEC in the left atrial appendage were respectively 97%, 100%, 100%, and 97%. (22)

Table 2.2. Comparison of Iodine and Blood Densities and Differences in Densities between the Regions of the LAA Thrombi and Pectinate Muscles and their Respective LAA Cavities in Patients with and without LAA Thrombi (He Y-Q, Liu L, Zhang M-C, Zeng H, Yang P. Dual-Energy Computed Tomography-Enabled Material Separation in Diagnosing Left Atrial Appendage Thrombus. Texas Heart Institute Journal. 2019;46(2):107-14.)(22)

	Group 1 (n=12)			Group 2 (n=12)			
Variable	LAA Cavities (mg/cm^3)	Pectinate Muscles (mg/cm^3)	*P* Value	LAA Cavities (mg/cm^3)	LAA Thrombi (mg/cm^3)	*P* Value	*P* Value*
Blood density	1,047.53 ± 11.88	1,002.37 ± 20.6	<0.001	1,046.74 ± 10.68	1,036.25 ± 24.87	0.192	0.001
Iodine density	16.64 ± 3.06	5.74 ± 2.4	<0.001	16.96 ± 4.83	1.77 ± 1.53	<0.001	<0.001
Blood-density differences	—	41.28 (34.5–47.69)	—	—	9.55 (–0.08 to 23.84)	—	0.003
Iodine-density differences	—	10.74 ± 2.14	—	—	15.19 ± 4.65	—	0.006

LAA = left atrial appendage

*LAA thrombi vs pectinate muscles

The blood-density differences were calculated by subtracting the blood densities in the central regions of the LAA pectinate muscles and thrombi from those of their respective LAA cavities for every slice. The iodine-density differences were calculated by subtracting the iodine densities in the central regions of the LAA pectinate muscles and thrombi from those of their respective LAA cavities for every slice.

Data are presented as mean ± SD or as median (25th–75th percentile). *P* <0.05 was considered statistically significant.

Spectral CT helps differentiate between left atrial thrombosis and pectinate muscle in the atrium, reconstructs the anatomy of the left atrium and pulmonary veins, and integrates CT images with electrophysiological maps, guiding for isolating pulmonary veins in atrial fibrillation ablation.

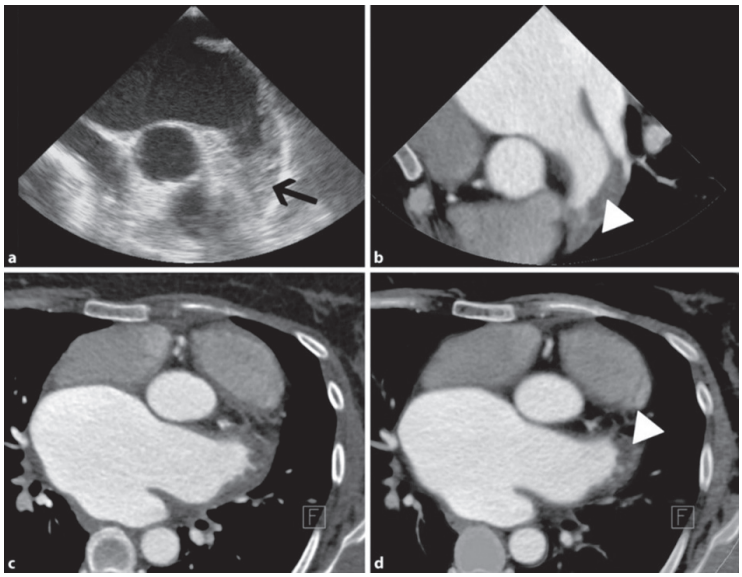


Figure 2.12. Dual-energy CT and SATTQ in a patient with left atrial appendage thrombosis. Thrombosis identified by transesophageal echocardiography; (a, arrow) and corresponding spectral CT images (b, arrowhead). Axial CT spectral images of the same patient show thrombus in the left atrium (c and d, arrows) (Source: Schlett, C. L., Heidt, M. C. et al. (2020). Mehrwert der Dual- Energy-Computertomographie zur Detektion von Thromben des linken Vorhofohrs Der Radiologe, 60(12).)(24)

III. CONCLUSION

The advent of spectral computed tomography that distinguishes materials with different effective atomic numbers has created many clinical applications. Spectral computed tomography is an imaging tool to investigate the degree of coronary stenosis and has a hemodynamic significance in examining myocardial perfusion as a functional diagnosis. Computed tomography (CT) scans help detect unstable plaques and predict the risk of acute cardiovascular events.

Computed tomography (CT) can be used as an initial diagnostic modality in patients at low or moderate risk for coronary artery disease.

Although magnetic resonance imaging remains the most optimal diagnostic modality for myocarditis and cardiomyopathies, spectral computed tomography can also diagnose these cases.

Investigating coronary stent restenosis or aortic stent Graft is also an advantage of spectral computed tomography.

The diagnosis of pulmonary embolism is based on the location of the embolized pulmonary artery, and the image of the lung parenchyma is evident and impressive with the color spectrum.

Computed tomography spectroscopy also helps to detect left atrial appendage thrombosis and create an electrophysiological map before atrial fibrillation; the radiation dose and the amount of contrast used in the patient are significantly reduced.

Abbreviation: HU: Hounsfield Units, SI: Signal Intensity, CT: Computed Tomography CTA: Computed Tomographic Angiography, MRI: Magnetic Resonance Imaging, DECT: Dual-energy computed tomography.

REFERENCES

1. Pim J de Feyter GPK, Filippo Cademartiri, Carlos van Mieghem, Bob Meijboom, Nico Mollet, Koen Nieman, Denise Vrouenraets. Computed Tomography of the Coronary Arteries. 2nd ed. CRC Press2008. 1-27 p.

2. Blankstein R. Cardiac Computed Tomography - Braunwald's Heart Disease: A Textbook of Cardiovascular Medicine: Elsevier Inc.; 2022. 335-62 p.

3. Achenbach S, Ulzheimer S, Baum U, Kachelrieß M, Ropers D, Giesler T, et al. Noninvasive coronary angiography by retrospectively ECG-gated multislice spiral CT. Circulation. 2000;102(23):2823-8.

4. Achenbach S, Giesler T, Ropers D, Ulzheimer S, Derlien H, Schulte C, et al. Detection of coronary artery stenoses by contrast-enhanced, retrospectively electrocardiographically-gated, multislice spiral computed tomography. Circulation. 2001;103(21):2535-8.

5. Schoepf UJ. CT of the Heart: Humana Totowa, NJ; 2005. 45-332 p.

6. McCollough CH, Leng S, Yu L, Fletcher JG. Dual-and multi-energy CT: principles, technical approaches, and clinical applications. Radiology. 2015;276(3):637-53.

7. Kaza RK, Platt JF, Cohan RH, Caoili EM, Al-Hawary MM, Wasnik A. Dual-energy CT with single- and dual-source scanners: current applications in evaluating the genitourinary tract. Radiographics. 2012;32(2):353-69.

8. Carrascosa PM, Garcia MJ, Cury RC, Leipsic JA. Dual Energy CT: Springer; 2015. 3-246 p.

9. Rassouli N, Etesami M, Dhanantwari A, Rajiah P. Detector-based spectral CT with a novel dual-layer technology: principles and applications. Insights into imaging. 2017;8:589-98.

10. Danad I, Fayad ZA, Willemink MJ, Min JK. New applications of cardiac computed tomography: dual-energy, spectral, and molecular CT imaging. JACC: Cardiovascular Imaging. 2015;8(6):710-23.

11. Patel AR, Bamberg F, Branch K, Carrascosa P, Chen M, Cury RC, et al. Society of cardiovascular computed tomography expert consensus document on myocardial computed tomography perfusion imaging. Journal of cardiovascular computed tomography. 2020;14(1):87-100.

12. Ohta Y, Kitao S, Yunaga H, Fujii S, Mukai N, Yamamoto K, et al. Myocardial delayed enhancement CT for the evaluation of heart failure: comparison to MRI. Radiology. 2018;288(3):682-91.

13. Kalisz K, Halliburton S, Abbara S, Leipsic JA, Albrecht MH, Schoepf UJ, et al. Update on cardiovascular applications of multi-energy CT. Radiographics. 2017;37(7):1955-74.

14. Adeboye A, Alkhatib D, Butt A, Yedlapati N, Garg N. A review of the role of imaging modalities in the evaluation of viral myocarditis with a special focus on COVID-19-related myocarditis. Diagnostics. 2022;12(2):549.

15. Carrascosa PM, Cury RC. Dual-Energy CT in Cardiovascular Imaging. 2015:173-230.

16. Cury RC, Leipsic J, Abbara S, Achenbach S, Berman D, Bittencourt M, et al. CAD-RADS™ 2.0–2022 Coronary Artery Disease-Reporting and Data System: An Expert Consensus Document of the Society

of Cardiovascular Computed Tomography (SCCT), the American College of Cardiology (ACC), the American College of Radiology (ACR), and the North America Society of Cardiovascular Imaging (NASCI). Cardiovascular Imaging. 2022;15(11):1974-2001.
17. Bratke G, Hickethier T, Bar-Ness D, Bunck AC, Maintz D, Pahn G, et al. Spectral photon-counting computed tomography for coronary stent imaging: evaluation of the potential clinical impact for the delineation of in-stent restenosis. Investigative radiology. 2020;55(2):61-7.
18. Sommer WH. 2011. 61-90 p.
19. Kassem TW. Follow up CT angiography post EVAR: Endoleaks detection, classification and management planning. The Egyptian Journal of Radiology and Nuclear Medicine. 2017;48(3):621-6.
20. Vlahos I, Jacobsen MC, Godoy MC, Stefanidis K, Layman RR. Dual-energy CT in pulmonary vascular disease. The British Journal of Radiology. 2022;95(1129):20210699.
21. Hong YJ, Hur J, Han K, Im DJ, Suh YJ, Lee H-J, et al. Quantitative analysis of a whole cardiac mass using dual-energy computed tomography: comparison with conventional computed tomography and magnetic resonance imaging. Scientific reports. 2018;8(1):15334.
22. He Y-Q, Liu L, Zhang M-C, Zeng H, Yang P. Dual-Energy Computed Tomography-Enabled Material Separation in Diagnosing Left Atrial Appendage Thrombus. Texas Heart Institute Journal. 2019;46(2): 107-14.
23. Sharma K, Brinker JA, Henrikson CA. Computed tomography imaging in atrial fibrillation ablation. Journal of Atrial Fibrillation. 2011;4(1).
24. Schlett C, Heidt M, Jörg A, Soschynski M, Buss S, Korosoglou G, et al. Mehrwert der Dual-Energy-Computertomographie zur Detektion von Thromben des linken Vorhofohrs. Der Radiologe. 2020;60(12).